Available online at www.sciencedirect.com

ScienceDirect

www.elsevier.com/locate/jes

JES JOURNAL OF ENVIRONMENTAL SCIENCES

www.jesc.ac.cn

Preparation of Ti species coating hydrotalcite by chemical vapor deposition for photodegradation of azo dye

Gaofei Xiao, HongYan Zeng, Sheng Xu, ChaoRong Chen, Quan Zhao, XiaoJun Liu*

College of Chemical Engineering, Xiangtan University, Xiangtan 411105, Hunan, China

ARTICLE INFO

Article history:
Received 8 December 2016
Revised 17 January 2017
Accepted 8 March 2017
Available online 28 March 2017

Keywords:
Chemical vapor deposition
Photocatalysis
Hydrotalcite
Ti species

ABSTRACT

TiO_2 in anatase crystal phase is a very effective catalyst in the photocatalytic oxidation of organic compounds in water. To improve its photocatalytic activity, the Ti-coating MgAl hydrotalcite (Ti–MgAl–LDH) was prepared by chemical vapor deposition (CVD) method. Response surface method (RSM) was employed to evaluate the effect of Ti species coating parameters on the photocatalytic activity, which was found to be affected by the furnace temperature, N_2 flow rate and influx time of precursor gas. Application of RSM successfully increased the photocatalytic efficiency of the Ti–MgAl–LDH in methylene blue photodegradation under UV irradiation, leading to improved economy of the process. According to the results from X-ray diffraction, scanning electron microscopy, Brunner–Emmet–Teller and Barrett–Joyner–Hallender, thermogravimetric and differential thermal analysis, UV–vis diffuse reflectance spectra analyses, the Ti species (TiO_2 or/and Ti^{4+}) were successfully coated on the MgAl–LDH matrix. The Ti species on the surface of the Ti–MgAl–LDH lead to a higher photocatalytic performance than commercial TiO_2-P25. The results suggested that CVD method provided a new approach for the industrial preparation of Ti-coating MgAl–LDH material with good photocatalytic performances.

Introduction

Color is one of the most obvious indicators of wastewater pollution. The discharges of highly colored dye effluent can indeed pollute the receiving water bodies. Due to its complex structure, it is very difficult to successfully treat using traditional biological processes (Han et al., 2016; Espantaleon et al., 2003). Therefore, the treatment of the effluent containing these compounds is important for the protection of natural waters. Traditional physical techniques, such as adsorption (Ghosh and Bhattacharyya, 2002; Zhu et al., 2015, 2016; Liu et al., 2016), coagulation by chemical agents and ion exchange on synthetic adsorbent resins (Monvisade and Siriphannon, 2009; Poon et al., 1999), have only limited success, since these methods merely transfer dye from water to solid, thus causing secondary pollution. Traditional chemical methods such as chlorination and ozonation are also used for the removal of certain dyes but being economically unfeasible and involving complicated procedures (Han et al., 2016; Konstantinou and Albanis, 2004). Advanced oxidation processes (AOPs) are alternative methods for the complete degradation of dye (Stylidi et al., 2003; Xu et al., 2014). Among AOPs, heterogeneous photocatalysis using TiO_2 as photocatalyst has proved to be an efficient tool for the degradation of the organic pollutants in aqueous solutions, since TiO_2 photocatalyst is largely available, inexpensive, non-toxic and shows relatively high chemical stability (Konstantinou and Albanis, 2004; Stylidi et al., 2003; Xu et al., 2014; Nakabayashi and Nosaka, 2013; Peng et al., 2005). The

* *Corresponding author.*
E-mail addresses: mgaofei@foxmail.com (G. Xiao), hyzeng@xtu.edu.cn (H. Zeng).

http://dx.doi.org/10.1016/j.jes.2017.03.031
1001-0742/

utilization from immobilizing or "supporting" Ti species onto a high-surface area support material has been found to enhance the photocatalytic efficiency for the ultraviolet lamp irradiation photooxidation of dye in comparison with neat TiO_2 (Konstantinou and Albanis, 2004; Xu et al., 2010; Scuderi et al., 2014; Matthews, 1991). A variety of materials including perlite (Hosseini et al., 2007), active carbon (Puma et al., 2008), polystyrene (Fabiyi and Skelton, 2000), silica (Aguedach et al., 2005) and clay (Feng et al., 2004; Hadjltaief et al., 2016), have been reported to be adopted as the supports. Among these, hydrotalcite-like materials (layer double hydroxide), a class of anionic clay minerals, are a promising alternative in view of its advantages including high porosity, high-surface area, high photostability, and suitability to work at ambient temperature (Han et al., 2016; Zeng et al., 2014a, 2014b; Mohapatra and Parida, 2016). Thus, loading TiO_2 on a hydrotalcite support is expected to enhance photodegradation owing to its ability to concentrate organic pollutants on the catalyst surface, by adsorption. Several preparation methods for Ti-coating hydrotalcite catalysts were used, which include reconstruction–impregnation (Seftel et al., 2013; Huang et al., 2013), coprecipitation–reconstruction (Seftel et al., 2013; Lu et al., 2012) and coprecipitation methods (Shao et al., 2014; Lu et al., 2012). It is fairly difficult to obtain evenly dispersing Ti species on the surface of a support using these methods, while they are not suitable for mass production (Yu et al., 2014). Chemical vapor deposition (CVD) is another good potential method for the preparation of high-dispersing Ti species materials, since the CVD method is effective for coating TiO_2 on a substrate with a flat smooth surface (Li et al., 2008), *i.e.*, layer double hydroxide. CVD offers significant advantages, due to its inherent versatility and the possibility of operating under relatively mild conditions (Ding et al., 2000; Tang et al., 2014). Up to now, rarely research reports about fabricating Ti species on the surface of hydrotalcites are available.

As the process of Ti species coating on the surface of hydrotalcites using CVD method is not a simple and single chemical process, it is indispensable to understand the optimal working conditions to enhance the methylene blue removal efficiency. The traditional "one-factor-at-a-time approach" is an operation frequently used in optimization to obtain high yields of the desired products. But the method disregards the complex interactions among various physico-chemical parameters. The response surface methodology (RSM) is a powerful statistical technique for optimizing experimental conditions and investigation of critical processes which can evaluate multiple parameters and their interactions by reducing the number of experimental trials, and also predicts their behavior under given sets of conditions (Pan et al., 2016).

In the present study, the CVD method was carried out for the synthesis of the Ti-coating MgAl hydrotalcite. The aim is to evaluate the potential application of the synthesized Ti-coating MgAl hydrotalcite catalyst for the photocatalytic degradation of methylene blue as a target compound. For the Ti species coating by CVD method, the parameters were investigated in detail based on the efficiency for the photodegradation of methylene blue by the Ti-coating MgAl hydrotalcite catalysts. The physico-chemical properties of the Ti-coating MgAl hydrotalcite catalysts were characterized according to the results from X-ray diffraction (XRD), scanning electron microscopy (SEM), Brunner–Emmet–Teller (BET) and Barrett–Joyner-Hallender (BJH), thermogravimetric and differential thermal analysis (TG-DTA), and UV–vis diffuse reflectance spectra (UV–vis DRS) analyses in order to clarify the relationship between the properties and catalytic performance.

1. Experimental

1.1. Materials

TiO_2-P25 (80% anatase and 20% rutile, average surface area of 50 m^2/g, size 20–30 nm) was purchased from Degussa Company, Essen, Germany. Methylene blue was purchased from Beijing Yili Chemical Co., Ltd., Beijing, China. Titanium tetrachloride ($TiCl_4$, 99.9%) and all other chemicals were of analytical grade and used without further purifications, which were purchased from Sinopharm Chemical Reagent Co. Ltd., Shanghai, China. All solutions were prepared with deionized water. The 0.1 mol/L NaOH and HCl solutions were used for pH adjustment. A pH electrode (Mettler-Toledo, S40 SevenMulti™, Greifensee, Switzerland) was used for pH measurements.

1.2. Preparation of MgAl hydrotalcite precursor

Mg/Al–CO_3^{2-} hydrotalcite precursor with Mg/Al molar ratio of 4.0 was prepared by urea hydrolysis according to the literature previously described (Zeng et al., 2009). An aqueous solution containing of $Mg(NO_3)_2{\cdot}6H_2O$ (0.12 mol/L) and $Al(NO_3)_3{\cdot}9H_2O$ (0.03 mol/L) was prepared, and urea ([urea]/[NO_3^-] molar ratio of 4.0) was dissolved in the above solution. The mixture was maintained at 105°C for 12 hr under stirring (300 r/min), and then aged statically at 90°C for 18 hr. The formed solid was collected by filtration, and then washed to neutral using deionized water. In the end, it was dried at 100°C for 12 hr, which was denoted as MgAl–LDH.

1.3. Preparation of the Ti-coating hydrotalcite

The Ti-coating hydrotalcite catalyst was prepared by CVD method, where $TiCl_4$ was used as Ti resource. CVD reactor was a homemade cold-wall system from the School of Chemical Engineering, Xiangtan University, and shown in Scheme 1. First, the MgAl–LDH nanoparticles of 4.0 g were placed in the center of the quartz tube furnace, and then N_2 flow was introduced in the reaction furnace for 10 min. Second, the furnace temperature was preheated from room temperature to a specific temperature (200–300°C) under pure N_2 atmosphere at a heating rate of 10°C/min for 2 hr. At the same time, 10 mL $TiCl_4$ in the reservoir was heated to 150°C, where $TiCl_4$ vapored. Then, the precursor gas, namely, $TiCl_4$ plus N_2 was introduced into the furnace, where N_2 was bubbled through a $TiCl_4$ reservoir at a given flux of 60–100 mL/min, and Ti species were deposited onto the surface of the MgAl–LDH. After the set time, the $TiCl_4$ gas was stopped, and the N_2 gas was kept flowing in the furnace for 2 hr to allow the $TiCl_4$ gas remain in the furnace reacts completely. Finally, the furnace was cooled slowly in pure N_2 to room temperature, and the resulting Ti-coating hydrotalcite was obtained. For convenience, the resulting Ti-coating hydrotalcite prepared under optimal conditions of

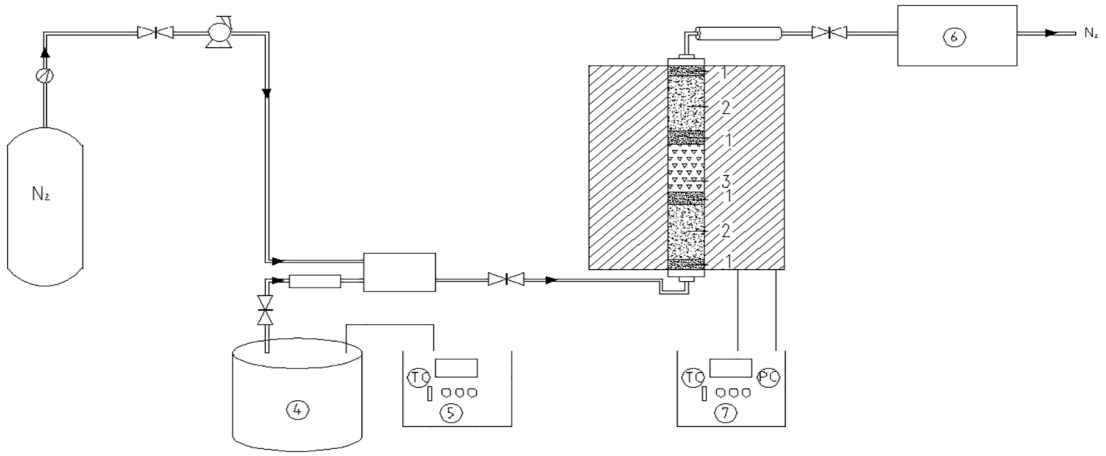

Scheme 1 – Experimental setup of the Ti-coating hydrotalcite catalyst was prepared using CVD method. (1) Quartz fiber; (2) Quartz sand; (3) MgAl–LDH particles; (4) $TiCl_4$ reservoir; (5) Control panel; (6) Tail gas absorption; (7) Control panel. CVD: chemical vapor deposition.

furnace temperature 260°C, precursor gas into the furnace of 6 hr and N_2 flow rate 90 mL/min, was denoted as Ti–MgAl–LDH.

1.4. Photocatalytic test

The photocatalytic test was carried out using methylene blue as test molecule. The UV irradiation source was a 300 W high-pressure mercury lamp (Institute of Electric Light Source, Beijing, China). Two hundred milligrams of catalyst was dispersed into 300 mL solution containing 1×10^{-5} mol/L of methylene blue, and the dispersion was maintained in dark with continuous sitting for 30 min, in order to reach the adsorption–desorption equilibrium. The suspension was then exposed to UV irradiation for 60 min. At 10 min interval, 3 mL of the reaction solution was withdrawn by a syringe. The reaction solution was centrifuged at 10000 r/min for 15 min. The supernatant was kept for methylene blue measurement by the spectrophotometric method (UV-2910, Hitachi, Japan) at 665 nm. A blank reaction was carried out under the same reaction conditions without adding any catalyst. All the experiments were carried out in triplicate under the same condition and average values are reported.

After approximation of the best conditions by "one-factor-at-a-time" method in our preliminary experiments for the methylene blue degradation by the Ti-coating hydrotalcite catalysts after 60 min, RSM was used to test the effect of preparation conditions, *i.e.*, furnace temperature (T, °C), time of precursor gas into the furnace (t, hr) and N_2 flow rate (F, mL/min), on the residue amount of methylene blue (η) in the methylene blue photocatalytic degradation for 60 min. The optimized response variable was the residue amount of methylene blue (η), and Box–Behnken Design (BBD) was used to design the experiments in Table 1. After the reaction, the response η was measured. The statistical software package Design Expert software (version 8.0.6) was used for the regression analysis of experimental data and to plot response surface. The second-order polynomial model was applied to predict the response variable (η) as shown below.

$$\eta = \beta_0 + \sum_{i=1}^{3} \beta_i X_i + \sum_{i=1}^{3} \beta_{ii} X_i^2 + \sum_{i}^{2} \sum_{j=i+1}^{3} \beta_{ij} X_i X_j \quad (1)$$

where, η was the response value (residue amount of methylene blue), β_0, β_i, β_{ii} and β_{ij} were the regression coefficients for interception, linear, quadratic and interaction terms, respectively. X_i and X_j were the independent variables.

1.5. Characterization

XRD patterns were collected on a Japan Rigaku D/max 2550PC (λ = 1.5405 Å) with CuKα radiation. The scan step was 0.1667°/sec with a filament intensity of 30 mA and a voltage of 40 kV. SEM (JSM-6700F, JEOL, Tokyo, Japan) at an accelerating voltage of 10 kV. The pore size distribution was calculated from desorption isotherm by the BJH method, and the specific surface area was calculated using the BET (NOVA-e1000, Quantachrome, USA) method based on the N_2 adsorption. TG-DTA (Mettler-Toledo, Zurich, Switzerland) was carried out in a nitrogen atmosphere with a heating rate of 10°C/min under a He stream flowing at 60 mL/min. The UV–visible diffuse reflectance spectra were recorded by spectrophotometer (Shimadzu UV-2550, Kyoto, Japan). The range of wavelength was 200–800 nm.

2. Results and discussion

2.1. Optimization of the CVD parameters by RSM

2.1.1. Analysis of the model

According to the BBD design of RSM, the methylene blue residue amounts obtained from all the experiments were

Table 1 – Levels of the independent variables used in the experimental design.

Independent variable	Symbol	Code level		
		−1	0	1
N_2 flow rate	F (mL/min)	60	80	100
Furnace temperature	T (°C)	200	250	300
Influx time of precursor gas	t (hr)	3	5	7

Table 2 – Experimental design with experimental and predicted values of methylene blue residue ratio.

Run	Experimental variables			Response η ($\times 10^{-5}$ mol/L)	
	F (mL/min)	t (hr)	T (°C)	Expt.	Predicted
1	80	3	200	0.44	0.43
2	80	5	250	0.14	0.13
3	80	7	300	0.10	0.10
4	100	3	250	0.28	0.28
5	100	5	200	0.25	0.25
6	80	5	250	0.14	0.13
7	80	5	250	0.13	0.12
8	80	7	200	0.25	0.25
9	60	3	250	0.43	0.43
10	100	5	300	0.12	0.11
11	80	3	300	0.24	0.24
12	60	5	300	0.21	0.20
13	60	7	250	0.25	0.25
14	60	5	200	0.46	0.46
15	80	5	250	0.13	0.12
16	80	5	250	0.11	0.13
17	100	7	250	0.11	0.11

listed in Table 2, where the center point in the design was repeated three times for the estimation of errors. The results of the second-order response surface model in the form of analysis of variance (ANOVA) by the software were given in Table 3. The model was a high significant with a p-value less than 0.0001 to predict the response values. The test variables T, F and t as well as F^2, T^2 and t^2 were highly significant with a p-value ($p < 0.0001$) to predict the response values, but Ft were insignificant ($p \geq 0.05$). The elimination of the insignificant term improved the regression model, and the quadratic model was given below,

$$\eta = 4.00 - 0.39F - 0.26t - 0.02T + 3.00 \times 10^{-5}FT + 1.50 \times 10^{-4}Tt + 1.72 \times 10^{-4}F^2 + 0.02T^2 + 2.45 \times 10^{-5}t^2 \quad (2)$$

where, T (°C) was the furnace temperature, t (hr) was the time of precursor gas into the furnace, and F (mL/min) was the N_2 flow rate. The goodness of fit of the model was examined by determination coefficient ($R^2 = 0.9973$), indicating that the sample variation of 99.73% was attributed to the independent variables and only 0.27% of the total variations were not explained by the model. As can be seen, the predicted values matched the experimental values reasonably well within the ranges of experimental conditions, with an R^2 value of 0.9916, demonstrating the applicability and reliability of the model over a range of experimental conditions with sufficient degree of accuracy. The adjusted R^2 (Adj $R^2 = 0.9939$) was also satisfactory to confirm the significance of the model. A relatively lower value of coefficient of variation (CV = 4.36%) suggested a good precision and reliability of the experiments (Pan et al., 2016). The non-significant value of lack of fit ($p > 0.05$) was good as the primary objective, implying that the model should fit the experimental data. ANOVA results of the quadratic model indicated that the quadratic model could be used to navigate the design space.

Table 3 – ANOVA analysis for response surface quadratic model ($\alpha = 0.05$).

Source	Sum of squares	Degree of freedom (DF)	Mean square	F	p-Value
Model	0.25	9	0.028	291.00	<0.0001
F	0.024	1	0.024	252.12	<0.0001
T	0.020	1	0.020	210.19	<0.0001
t	0.029	1	0.029	299.80	<0.0001
FT	0.00002	1	0.00002	37.33	<0.0001
Ft	0.00360	1	0.00360	0.26	0.6263
Tt	0.00020	1	0.00020	21.00	0.0005
F^2	0.018	1	0.018	184.48	<0.0001
T^2	0.022	1	0.022	229.51	<0.0001
t^2	0.018	1	0.018	184.48	<0.0001
Residual	0.00067	7	0.00009		
Lack of fit	0.00075	3	0.00005	0.17	0.9136
Pure error	0.0006	4	0.00015		
Core total	0.25	16			
R^2	0.9973				
Adjusted R^2	0.9939				
Predicted R^2	0.9916				
Adeq precision	49.4590				
Coefficient of variation	4.36%				

ANOVA: analysis of variance.

2.1.2. Interactions between the variables

Based on the ANOVA results, furnace temperature was found to have the greatest significant effect on methylene blue degradation, while there was a highly significant interaction on the response between furnace temperature and N_2 flow rate as well as between furnace temperature and influx time of precursor gas. Therefore, it was of great interest to further investigate the interactive effects of the variables in the range of experimental conditions. Fig. 1a showed the interactive effect of furnace temperature and N_2 flow rate on methylene blue residue amount, while influx time of precursor gas was fixed at zero level, *i.e.*, 5 hr. It was clear that the interactive effect of furnace temperature and N_2 flow rate was significant with the contour curve of oval shape. The furnace temperature demonstrated a quadratic effect on the response, where methylene blue residue amount decreased with furnace temperature up at lower temperature (<260°C), followed by a gradual increase with an increase in furnace temperature. At the same time, methylene blue residue amount decreased with the increasing N_2 flow rate, and then sunk to a low level as N_2 flow rate was increased above 90 mL/min. As shown in Fig. 1b, the furnace temperature–influx time of precursor gas interaction was significant with the contour curve of oval shape. The furnace temperature also demonstrated a quadratic effect on the response, where residue amount declined to about 0.07×10^{-5} mol/L at 260°C, followed by an elevation with increase in temperature. Meanwhile, methylene blue residue amount exerted a downward trend with increasing the influx time of precursor gas, and then achieved a balance with further extending the time (>6 hr).

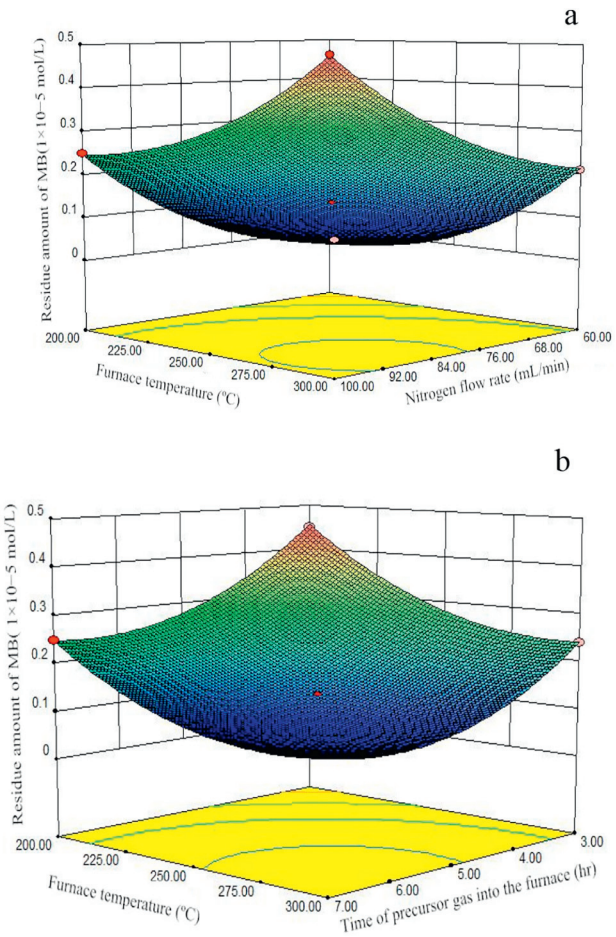

Fig. 1 – Interactive effect between furnace temperature and N_2 flow rate towards methylene blue residue amount (a), and interactive effect between furnace temperature and influx time of precursor gas towards methylene blue residue amount (b).

2.1.3. Optimization of CVD process parameters

In this study, the optimization of the methylene blue degradation process using Design Expert 8.0.5 software was performed for an optimum combination of CVD parameters to give minimum methylene blue residue amount. The model predicted the minimum methylene blue residue amount appeared at furnace temperature 260°C, influx time of precursor gas for 6 hr and N_2 flow rate 90 mL/min, respectively. The theoretical methylene blue residue amount which was predicted under the above conditions was 0.07×10^{-5} mol/L.

Additional experiment was carried out to validate the optimization result obtained by RSM under the optimal state conditions of furnace temperature 260°C, influx time of precursor gas for 6 hr and N_2 flow rate 90 mL/min, and the experiment was repeated five times for the estimation of errors. It was observed that the experimental methylene blue residue amount (0.07×10^{-5} mol/L, $\sigma = 0.0001$) was fitted to the predicted value from the model, which had a relatively small error (0.01%) between the predicted and the experimental value. These results confirm the predictability and efficacy of the model for the methylene blue residue amount in the experimental conditions. On the other hand, the sample prepared under the optimal CVD conditions was chosen for the following analyses, which donated as Ti–MgAl–LDH.

2.2. Ti–MgAl–LDH photocatalytic activities

Under UV irradiation conditions, the activities of the Ti–MgAl–LDH, MgAl–LDH and TiO_2-P25 catalysts were investigated to determine the Ti–MgAl–LDH suitability for the degradation of methylene blue. At the same time, the blank reaction as control was also carried out under the same reaction conditions without adding any catalyst, and the results were shown in Fig. 2. As seen in Fig. 2, the methylene blue residue amounts were quite high in dark adsorption process for the preprocessing 30 min, which were higher than 0.97×10^{-5} mol/L of methylene blue close to the initial methylene blue concentration, 1×10^{-5} mol/L). The result demonstrated that the methylene blue adsorption on the catalysts was nearly negligible. On the other hand, UV photolysis alone degraded very little methylene blue with high residue amount 0.92×10^{-5} mol/L, while the addition of photocatalysts accelerated the methylene blue degradation. The MgAl–LDH precursor demonstrated a very low photocatalytic activity, where the residue amount of methylene blue was still 0.33×10^{-5} mol/L after 60 min of UV irradiation. Compared to the TiO_2-P25, the Ti–MgAl–LDH indicated a significant enhanced photocatalytic activity (0.09×10^{-5} mol/L) with high mineralization efficiency. The catalytic activity of the three samples was in the following sequence: Ti–MgAl–LDH > TiO_2-P25 > MgAl–LDH.

The photocatalytic reaction kinetics was usually described by the pseudo-second-order model due to their good representation of the experimental data for photocatalytic reaction systems. A simple reaction rate expression was performed with the aid of pseudo-second-order equation as follows (Chen and Li, 2010; Hsieh et al., 2009; Velasco et al., 2010),

$$\frac{t}{q_t} = \frac{1}{kq_e^2} + \frac{1}{q_e} \tag{3}$$

where, k ((L·min)/mg) was the reaction rate constant of second-order adsorption, and q_t ((L·min)/mg) and q_e ((L·min)/mg) were the amount of the methylene blue degradation at t (min) time and equilibrium, respectively.

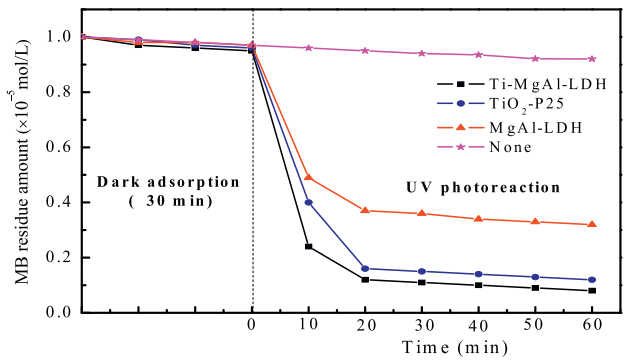

Fig. 2 – The behavior of the Ti–MgAl–LDH, MgAl–LDH and TiO_2-P25 catalysts in the photodegradation of methylene blue under ultraviolet (UV) irradiation.

Table 4 – Photocatalytic kinetic parameters.

	k ((L·min)/mg)	h (mg/(L·min))	R^2
TiMgAl–LDH	0.01815	0.01638	0.998
TiO_2-P25	0.01629	0.01564	0.986
MgAl–LDH	0.01328	0.00669	0.996
Photolysis	0.00695	0.00006	0.978

For the data obtained in the present study (Fig. 2), the kinetic parameters were calculated according to pseudo-second-order model and the results were showed in Table 4. The results in Table 4 showed that the calculated correlation coefficient values for the model were higher than 0.986, implying that the pseudo-second-order model was suitable in describing the photocatalytic reaction process. In the pseudo-second-order model, the constant k could be used to calculate the initial reaction rate h, at $t \rightarrow 0$ (Velasco et al., 2010; Vadivelan and Kumar, 2005), as follow,

$$h = kq_e^{\ 2} \quad (4)$$

As in Table 4, the Ti–MgAl–LDH had maximum h value, followed by the TiO_2-P25, while the MgAl–LDH possessed the lowest h value, indicating that the Ti–MgAl–LDH had the highest photocatalytic activity due to Ti species coating on the surface of the MgAl–LDH precursor during CVD preparation. Thus, it would seem that the immobilization of Ti species on the surface of the MgAl–LDH support could improve the photocatalytic efficiency, leading to the good photocatalytic activity of the Ti–MgAl–LDH.

2.3. Photocatalyst characterization

2.3.1. XRD analyses

The powder XRD patterns of the Ti–MgAl–LDH and MgAl–LDH catalysts were shown in Fig. 3. The Ti–MgAl–LDH and MgAl–LDH LDH catalysts had the typical crystalline phase of pure hydrotalcite (JCPDS 21-1276) with sharp and intense (003), (006), (009), (110) and (113) reflections. The interlayer distance ($d_{003} \approx 0.77$ nm) was a typical of CO_3^{2-} intercalated hydrotalcite (Han et al., 2016; Zeng et al., 2009). The parameter a, the average cation–cation distance in the brucite sheets, could be calculated, $a = 2d(110)$, from the (110) XRD refection. The essentially similarity in the a value in the Ti–MgAl–LDH (0.304 nm) and MgAl–LDH (0.303 nm) indicated that the immobilization of Ti species did not change the microstructure of the brucite sheets of (Pausch et al., 1986). It was very interesting that four reflections (2θ = 25.2, 31.3, 41.5 and 51.4°) were revealed for the Ti–MgAl–LDH, belonging to the anatase-type TiO_2 (JCPDS 21-1276). Additionally, the reflections of anatase phase were relatively sharp and intense, indicating the high crystalline character of TiO_2 particles.

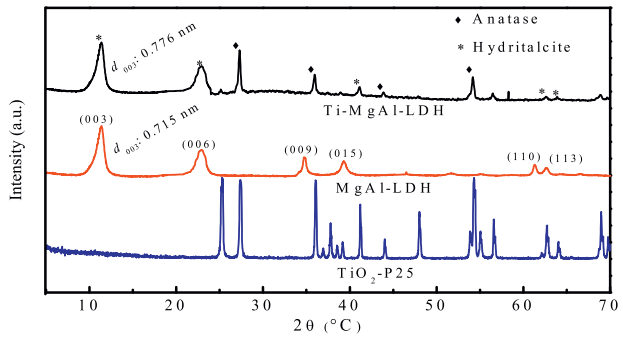

Fig. 3 – XRD spectra of the Ti–MgAl–LDH, MgAl–LDH and TiO_2-P25 catalysts. XRD: X-ray diffraction.

2.3.2. SEM analyses

The morphology of the Ti–MgAl–LDH and MgAl–LDH catalysts was monitored by SEM analysis as shown in Fig. 4. The Ti–MgAl–LDH and MgAl–LDH catalysts were made of thin flat crystals indicating the layered structure, which were in line with the typical hydrotalcite morphology with irregular edges. The MgAl–LDH indicated individually layered platelets with glossy surface, while the Ti–MgAl–LDH had some tendency for platelets to aggregate in a clumpy manner, possibly due to the formation of the anatase-type TiO_2 phase. Some of the particles could be seen transversely, allowing to estimate the platelet thickness. The platelet thickness of the Ti–MgAl–LDH was obviously thicker than that of the MgAl–LDH. In particular, the surface morphology of the Ti–MgAl–LDH particles appeared the TiO_2 nanoparticles homogeneously dispersed on the brucite sheets. The result could pin down the inference from the XRD analyses that there was the anatase-type TiO_2 crystalline on the surface of Ti–MgAl–LDH particles.

2.3.3. Textural analyses

In order to examine the textural characteristic of the catalysts, N_2 adsorption–desorption experiments were also studied to characterize the TiO_2 immobilization on the surface of Ti–MgAl–LDH particles. The adsorption isotherms of the Ti–MgAl–LDH and MgAl–LDH catalysts were basically similar and the plots shown in Fig. 5. The two samples displayed a typical IV isotherm with a H3 hysteresis loop according to the International Union of Pure and Applied Chemistry classification. The isotherm of the MgAl–LDH had a H3 hysteresis loop in high relative pressure range of 0.40–0.95, which presented a broad pore size distribution in broad mesoporous region due to the aggregates of plate-like particles, giving rise to slit-like pores with nonuniform size and almost without micropores (Parida et al., 2012). While after the TiO_2 immobilization, the isotherm displayed a remarkably capillary condensation step between 0.02 and 0.95 P/P_o. This demonstrated that the Ti–MgAl–LDH had a broad pore size distribution with mesoporous structures as well as a few micropores, possibly due to the TiO_2 crystalline on the brucite sheets. The significant adsorption at lower relative pressure was more likely because of monolayer coverage of the TiO_2 crystalline (Kresge et al., 1992). On the other hand, the Ti–MgAl–LDH and MgAl–LDH had a similar surface area (about 79 and 84 m^2/g), while the TiO_2-P25 also possessed a very close surface area (50 m^2/g). Such changes suggested that the anchorage of anatase-type TiO_2 crystalline on the surface of the brucite sheets induced the modification in the textural properties.

2.3.4. TG-DTA analyses

Thermogravimetric analysis (TG) was one of the thermal analysis techniques used to measure the physical chemistry properties of a material as a function of temperature or mass

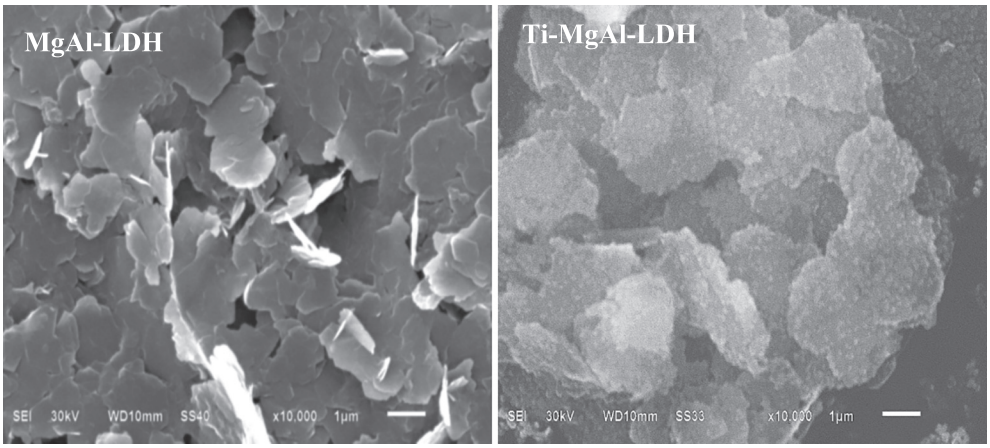

Fig. 4 – SEM images of the Ti–MgAl–LDH and MgAl–LDH catalysts. SEM: scanning electron microscopy.

loss. The effect of introduced Ti species on the MgAl–LDH matrix was investigated by thermogravimetric and differential thermal (TG/DTA) analysis, and the TG/DTA profiles were shown in Fig. 6, where there are significant differences between the Ti–MgAl–LDH and MgAl–LDH. The DTA curve of the MgAl–LDH showed three endothermic peaks. The first endothermic stage with 15.83% weight loss at about 200°C corresponded to the loss of physisorbed and interlayer water without collapse of hydrotalcite structure. The second stage with 10.09% weight loss centering at 300°C was due to the removal of hydroxyl groups from the brucite sheets as water vapor. And the last stage with 7.94% weight loss at around 425°C was due to the loss of the interlayer CO_3^{2-} anions (Rives, 2002). In contrast, the Ti–MgAl–LDH showed four endothermic peaks observed in the TGA profile at temperatures at 30–150, 150–200, 200–250 and 390–500°C. The first weight loss (13.38%) might be associated with the removal of physically adsorbed and intercalated water molecules. The second one (8.83%) was due to the liberation of surficial Ti–OH groups (Maslova et al., 2008; Zhang et al., 2014), and the third one (9.09%) corresponded to the dehydroxylation of the brucite-like sheets. The weight loss centered at 425°C with 13.13%, which was similar to that from the MgAl–LDH precursor, was still due to the removal of interlayer CO_3^{2-} anions. The decrease in temperature of the endothermic peak between 30 and 350°C revealed the weakening interaction, and the removals of physisorbed and interlayer water molecules as well as hydroxyl groups from the brucite sheets including Ti–OH groups became easier. The differences should be due to a complex decomposition mechanism for the Ti species coating on the MgAl–LDH. Therefore it can be concluded that Ti species existed on the surface of the brucite sheets not only in the anatase-type TiO_2 form but also the Ti–OH group (Ti^{4+}) form.

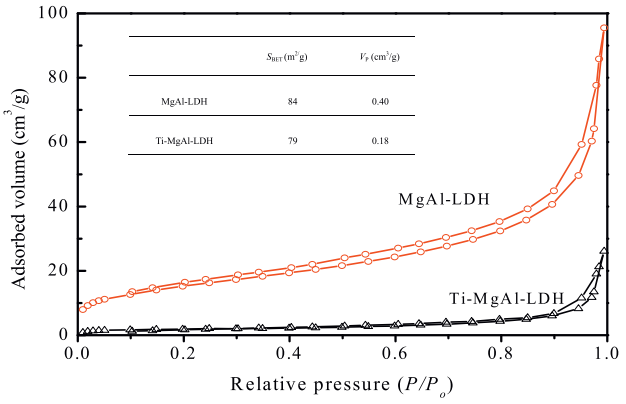

Fig. 5 – N_2 adsorption/desorption isotherms and corresponding textural properties (inset) for the Ti–MgAl–LDH and MgAl–LDH catalysts. S_{BET}: specific surface area, V_p: pore volume, D_p: average pore diameter.

2.3.5. UV–vis DRS analyses

UV–vis DRS measurement was a very simple method, which used as a sensitive measure of the possible changes in molecule structure of the materials. In the present study, it was used to investigate the environment and the coordination state of the Ti^{4+} in the obtained Ti–MgAl–LDH. The UV–vis DRS of the Ti–MgAl–LDH and MgAl–LDH catalysts were compared in Fig. 7. As seen in Fig. 7a, the MgAl–LDH precursor exhibited relatively low absorption below 250 nm. TiO_2-P25 showed an intense absorption band in the UV region below 385 nm originating from charge transfer that occurs between the 2p orbital of the oxygen atom to the 3d of the Ti. It could be due to the presence of the anatase-type TiO_2 (Yu et al., 2006) and/or Ti–O bond from the Ti–OH group on the surface of the brucite sheets (Dou et al., 2015). For the Ti–MgAl–LDH, the absorbance strongly increased in the UV region, showing similar optical characteristics to the TiO_2-P25. A significant red-shift was found, and the absorbance in the region 200–400 nm indicated the octahedral coordination of Ti atoms in the brucite-like sheets (Shao et al., 2011). Maximum absorption shifted to longer wavelength indicated that less energy would be necessary for photocatalytic activity.

In order to obtain details about light absorptive properties of the Ti–MgAl–LDH and MgAl–LDH, the band gap energies were estimated by the Tauc relation using the transformed Kubelka–Munk function according to the following equation (Lu et al., 2012):

$$\alpha E_p = K(E_p - E_g)^n \quad (5)$$

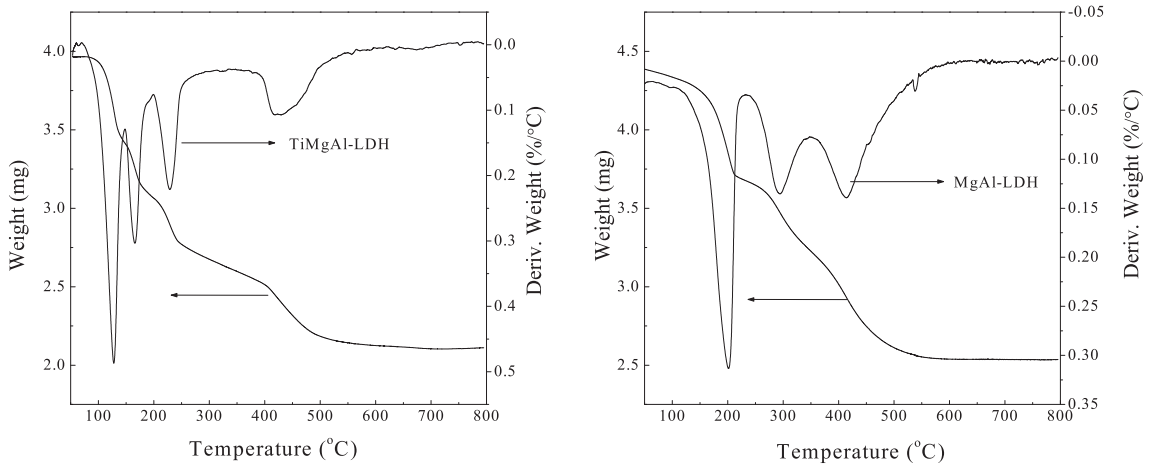

Fig. 6 – Thermogravimetric and differential thermal analysis (TG/DTA) curves of the Ti–MgAl–LDH and MgAl–LDH catalysts.

where, α was the absorption coefficient, E_g was the band gap, E_p was the optical band gap, K is a constant, and n depended on the nature of the transition. Among them, n depended on the type of optical transition in a semiconductor. The n values of 1/2, 3/2, 2 and 3 were corresponded to allow direct transitions, forbid direct transitions, allow indirect transitions, and forbid indirect transitions, respectively.

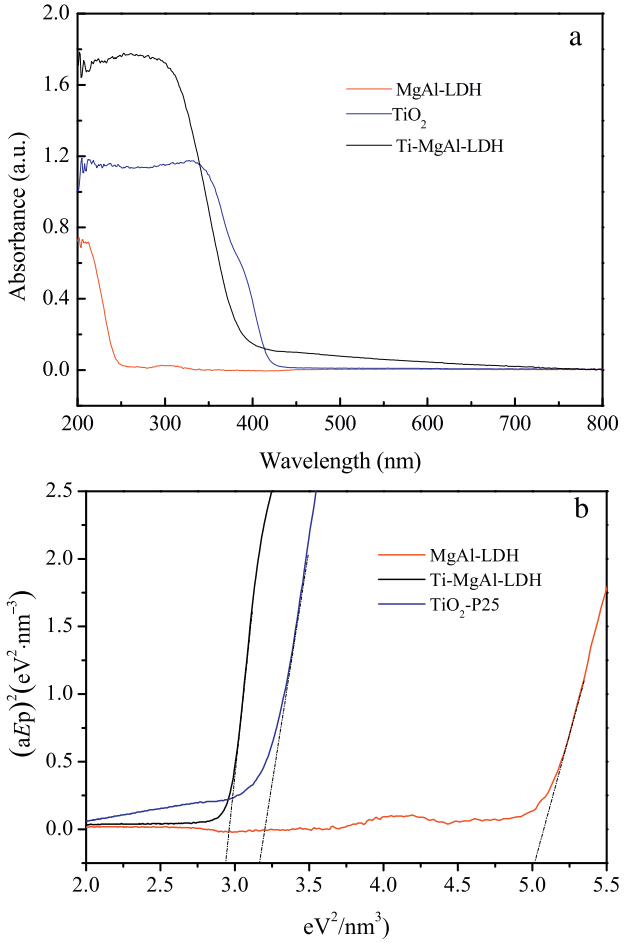

Fig. 7 – UV–Visdiffuse DRS (a) and Tauc plots (b) of $(\alpha E_p)^2$ *versus* E_p of the Ti–MgAl–LDH, MgAl–LDH and TiO_2-P25 catalysts. DRS: diffuse reflectance spectra.

The band gap energies of the Ti–MgAl–LDH and MgAl–LDH catalysts were shown in Fig. 7b. The n values of the Ti–MgAl–LDH and TiO_2-P25 were lesser than 1/2, it suggested that there were allowed direct transitions across the energy band gap. Nevertheless, it demonstrated that the absorption feature of the MgAl–LDH was attributed to forbid direct transitions, since the n value of the MgAl–LDH was 0.66. The result showed that the MgAl–LDH had lower photocatalytic activity. At the same time, the curves of $(\alpha E_p)^2$ *versus* E_p were plotted, as shown in Fig. 7b. The band gaps E_p were estimated to be 2.93, 5.0 and 3.17 eV for the Ti–MgAl–LDH, MgAl–LDH and TiO_2-P25, respectively. Comparing to the TiO_2-P25, the Ti–MgAl–LDH had been slightly lower E_p value (2.93 eV). The result indicated that the introduction of Ti species caused the change of the band gap, indicating that photocatalytic activity enhancement could be ascribed directly to the band gap. At the same time, the low band gap (<3.10 eV) accounted for its specific visible-light photocatalytic activity. So, there was good reason to deduce that the Ti species (anatase-type TiO_2 or/and Ti^{4+}) on the MgAl–LDH matrix enhanced the photocatalytic activity (Lu et al., 2012; Dou et al., 2015). The results suggested that the Ti–MgAl–LDH was an attractive photocatalyst candidate for industrialized environmental purification with high photocatalytic activity.

3. Conclusions

The fabrication and application of LDH-based photocatalysts represented a promising direction in the development of LDH-based multifunctional materials. In the present work, a facile and dynamic CVD process was employed to deposit the dispersing Ti species on the surface of the MgAl–LDH particles. The resulting Ti–MgAl–LDH material was examined as a photocatalyst for methylene blue degradation under UV irradiation. Optimization of the parameters for the immobilization of the Ti species on the MgAl–LDH precursor was carried out using RSM, where the second-order model showed a significant

precision to predict the response value (methylene blue residual amount). The optimum conditions – the furnace temperature, influx time of precursor gas and N_2 flow rate – were 260°C, 6 hr and 90 mL/min, which the predicted methylene blue residual amount was 0.09 mol/L.

Ti species in the form of the anatase-type TiO_2 and/or Ti–OH group (Ti^{4+}) on the MgAl–LDH matrix was confirmed by XRD, SEM, BET/BJH, TG/DTA and UV–vis DRS analyses. The Ti species dispersed on the surface of the MgAl–LDH enabled the photocatalytic activity, which was significantly higher than that of commercial TiO_2-P25 as well as the precursor MgAl–LDH.

Acknowledgments

This work was supported by the Hunan 2011 Collaborative Innovation Center of Chemical Engineering & Technology with Environmental Benignity and Effective Resource Utilization.

REFERENCES

Aguedach, A., Brosillon, S., Morvan, J., Lhadi, E.K., 2005. Photocatalytic degradation of azo-dyes reactive black 5 and reactive yellow 145 in water over a newly deposited titanium dioxide. J. Phys. Chem. B 57, 55–62.

Chen, Y.H., Li, F.A., 2010. Kinetic study on removal of copper(II) using goethite and hematite nano-photocatalysts. J. Colloid Interface Sci. 347, 277–281.

Ding, Z., Hu, X., Lu, G.Q., Yue, P.L., Greenfield, P.F., 2000. Novel silica gel supported TiO_2 photocatalyst synthesized by CVD method. Langmuir 16, 6216–6222.

Dou, Y., Zhang, S., Pan, T., Xu, S., Zhou, A., Pu, M., et al., 2015. TiO_2@layered double hydroxide core–shell nanospheres with largely enhanced photocatalytic activity toward O_2 generation. Adv. Funct. Mater. 25, 2243–2249.

Espantaleon, A.G., Nieto, J.A., Fernandez, M., Marsal, A., 2003. Use of activated clays in the removal of dyes and surfactants from tannery wastewaters. Appl. Clay Sci. 24, 105–110.

Fabiyi, M.E., Skelton, R.L., 2000. Photocatalytic mineralisation of methylene lue using buoyant TiO_2-coated polystyrene beads. J. Photochem. Photobiol. A Chem. 132, 121–128.

Feng, J., Wong, R.S.K., Hu, X., Yue, P.L., 2004. Discoloration and mineralization of orange II by using Fe^{3+}-doped TiO_2 and bentonite clay-based Fe nanocatalysts. Catal. Today 98, 441–446.

Ghosh, D., Bhattacharyya, K.G., 2002. Adsorption of methylene blue on kaolinite. Appl. Clay Sci. 20, 295–300.

Hadjltaief, H.B., Zina, M.B., Galvez, M.E., Da Costa, P., 2016. Photocatalytic degradation of methyl green dye in aqueous solution over natural clay-supported ZnO–TiO_2 catalysts. J. Photochem. Photobiol. A Chem. 315, 25–33.

Han, J., Zeng, H.Y., Xu, S., Chen, C.R., Liu, X.J., 2016. Catalytic properties of CuMgAlO catalyst and degradation mechanism in CWPO of methyl orange. Appl. Catal. A Gen. 527, 72–80.

Hosseini, S.N., Borghei, S.M., Vossoughi, M., Taghavinia, N., 2007. Immobilization of TiO_2 on perlite granules for photocatalytic degradation of phenol. Appl. Catal. B Environ. 74, 53–62.

Hsieh, C.T., Fan, W.S., Chen, W.Y., Lin, J.Y., 2009. Adsorption and visible-light-derived photocatalytic kinetics of organic dye on Co-doped titania nanotubes prepared by hydrothermal synthesis. Sep. Purif. Technol. 67, 312–318.

Huang, Z., Wu, P., Lu, Y., Wang, X., Zhu, N., Dang, Z., 2013. Enhancement of photocatalytic degradation of dimethyl phthalate with nano-TiO_2 immobilized onto hydrophobic layered double hydroxides: a mechanism study. J. Hazard. Mater. 246, 70–78.

Konstantinou, I.K., Albanis, T.A., 2004. TiO_2-assisted photocatalytic degradation of azo dyes in aqueous solution: kinetic and mechanistic investigations: a review. Appl. Catal. B Environ. 49, 1–14.

Kresge, C.T., Leonowicz, M.E., Roth, W.J., Vartuli, J.C., Beck, J.S., 1992. Ordered mesoporous molecular sieves synthesized by a liquid-crystal template mechanism. Nature 359, 710–712.

Li, G., Bai, R., Zhao, X.S., 2008. Coating of TiO_2 thin films on the surface of SiO_2 microspheres: toward industrial photocatalysis. Ind. Eng. Chem. Res. 47, 8228–8232.

Liu, J., Zhu, R.L., Xu, T.Y., Xu, Y., Ge, F., Xi, Y.F., et al., 2016. Co-adsorption of phosphate and zinc (II) on the surface of ferrihydrite. Chemosphere 144, 1148–1155.

Lu, R., Xu, X., Chang, J., Zhu, Y., Xu, S., Zhang, F., 2012. Improvement of photocatalytic activity of TiO_2 nanoparticles on selectively reconstructed layered double hydroxide. Appl. Catal. B Environ. 111, 389–396.

Maslova, M.V., Rusanova, D., Naydenov, V., Antzutkin, O.N., Gerasimova, L.G., 2008. Synthesis, characterization, and sorption properties of amorphous titanium phosphate and silica-modified titanium phosphates. Inorg. Chem. 47, 11351–11360.

Matthews, R.W., 1991. Photooxidative degradation of coloured organics in water using supported catalysts TiO_2 on sand. Water Res. 25, 1169–1176.

Mohapatra, L., Parida, K., 2016. A review on the recent progress, challenges and perspective of layered double hydroxides as promising photocatalysts. J. Mater. Chem. A 4, 10744–10766.

Monvisade, P., Siriphannon, P., 2009. Chitosan intercalated montmorillonite: preparation, characterization and cationic dye adsorption. Appl. Clay Sci. 42, 427–431.

Nakabayashi, Y., Nosaka, Y., 2013. OH radical formation at distinct faces of rutile TiO_2 crystal in the procedure of photoelectrochemical water oxidation. J. Phys. Chem. C 117, 23832–23839.

Pan, A.D., Zeng, H.Y., Alain, G.B.F.C., Feng, B., 2016. Heat-pretreatment and enzymolysis behavior of the lotus seed protein. Food Chem. 201, 230–236.

Parida, K., Mohapatra, L., Baliarsingh, N., 2012. Effect of Co^{2+} substitution in the framework of carbonate intercalated Cu/Cr LDH on structural, electronic, optical, and photocatalytic properties. J. Phys. Chem. C 116, 22417–22424.

Pausch, I., Lohse, H.H., Allmann, R., 1986. Syntheses of disordered and A1-rich hydrotalcite-like compounds. Clay Clay Miner. 34, 507–510.

Peng, T., Zhao, D., Dai, K., Shi, W., Hirao, K., 2005. Synthesis of titanium dioxide nanoparticles with mesoporous anatase wall and high photocatalytic activity. J. Phys. Chem. B 109, 4947–4952.

Poon, C.S., Huang, Q., Fung, P.C., 1999. Degradation kinetics of cuprophenyl yellow RL by UV/H_2O_2/ultrasonication (US) process in aqueous solution. Chemosphere 38, 1005–1014.

Puma, G.L., Bono, A., Krishnaiah, D., Collin, J., 2008. Preparation of titanium dioxide photocatalyst loaded onto activated carbon support using chemical vapor deposition: a review paper. J. Hazard. Mater. 157, 209–219.

Rives, V., 2002. Characterisation of layered double hydroxides and their decomposition products. Mater. Chem. Phys. 75, 19–25.

Scuderi, V., Impellizzeri, G., Romano, L., Scuderi, M., Nicotra, G., Bergum, K., et al., 2014. TiO_2-coated nanostructures for dye photo-degradation in water. Nanoscale Res. Lett. 9, 1–7.

Seftel, E.M., Mertens, M., Cool, P., 2013. The influence of the Ti^{4+} location on the formation of self-assembled nanocomposite systems based on TiO_2 and Mg/Al–LDHs with photocatalytic properties. Appl. Catal. B Environ. 134, 274–285.

Shao, M., Han, J., Wei, M., Evans, D.G., Duan, X., 2011. The synthesis of hierarchical Zn–Ti layered double hydroxide for efficient visible-light photocatalysis. Chem. Eng. J. 168, 519–524.

Shao, L., Yao, Y., Quan, S., Wei, H., Wang, R., Guo, Z., 2014. One-pot in situ synthesized TiO_2/layered double hydroxides (LDHs) composites toward environmental remediation. Mater. Lett. 114, 111–114.

Stylidi, M., Kondarides, D.I., Verykios, X.E., 2003. Pathways of solar light-induced photocatalytic degradation of azo dyes in aqueous TiO_2 suspensions. Appl. Catal. B Environ. 40, 271–286.

Tang, S., Wang, J., Zhu, Q., Chen, Y., Li, X., 2014. Preparation of rutile TiO_2 coating by thermal chemical vapor deposition for anticoking applications. ACS Appl. Mater. Interfaces 6, 17157–17165.

Vadivelan, V., Kumar, K.V., 2005. Equilibrium, kinetics, mechanism, and process design for the sorption of methylene blue onto rice husk. J. Colloid Interface Sci. 286 (1), 90–100.

Velasco, L.F., Parra, J.B., Ania, C.O., 2010. Role of activated carbon features on the photocatalytic degradation of phenol. Appl. Surf. Sci. 256, 5254–5258.

Xu, Y.J., Zhuang, Y., Fu, X., 2010. New insight for enhanced photocatalytic activity of TiO_2 by doping carbon nanotubes: a case study on degradation of benzene and methyl orange. J. Phys. Chem. C 114, 2669–2676.

Xu, D., Cheng, F., Lu, Q., Dai, P., 2014. Microwave enhanced catalytic degradation of methyl orange in aqueous solution over CuO/CeO_2 catalyst in the absence and presence of H_2O_2. Ind. Eng. Chem. Res. 53, 2625–2632.

Yu, X., Wu, Q., Jiang, S., Guo, Y., 2006. Nanoscale ZnS/TiO_2 composites: preparation, characterization, and visible-light photocatalytic activity. Mater. Charact. 57, 333–341.

Yu, J., Yang, J., Feng, X., Jia, H., Wang, J., Lu, W., 2014. Uniform carbon coating on silicon nanoparticles by dynamic CVD process for electrochemical lithium storage. Ind. Eng. Chem. Res. 53, 12697–12704.

Zeng, H.Y., Deng, X., Wang, Y.J., Liao, K.B., 2009. Preparation of Mg–Al hydrotalcite by urea method and its catalytic activity for transesterification. AIChE J 55, 1229–1235.

Zeng, H.Y., Zhu, P.H., Xu, S., Liao, M.C., Zhang, Z.Q., Liu, X.J., et al., 2014a. Preparation of ultrafine nanoparticles under super-gravity field and their flame-retardant properties. Ind. Eng. Chem. Res. 53, 18380–18389.

Zeng, H.Y., Xu, S., Liao, M.C., Zhang, Z.Q., Zhao, C., 2014b. Activation of reconstructed Mg/Al hydrotalcites in the transesterification of microalgae oil. Appl. Clay Sci. 91, 16–24.

Zhang, G., Sun, M., Liu, Y., Lang, X., Liu, L., Liu, H., et al., 2014. Visible-light induced photocatalytic activity of electrospun-TiO_2 in arsenic (III) oxidation. ACS Appl. Mater. Interfaces 7, 511–518.

Zhu, R.H., Chen, Q., Zhu, R.L., Xu, Y., Ge, F., Zhu, J.X., et al., 2015. Sequestration of heavy metal cations on montmorillonite by thermal treatment. Appl. Clay Sci. 107, 90–97.

Zhu, R.L., Chen, Q.Z., Zhou, Q., Xi, Y.F., Zhu, J.X., He, H.P., 2016. Adsorbents based on montmorillonite for contaminant removal from water: a review. Appl. Clay Sci. 123, 239–258.